Paper

Int'l J. of Aeronautical & Space Sci. 16(2), 223–246 (2015)
DOI: http://dx.doi.org/10.5139/IJASS.2015.16.2.223

IJASS
International Journal of Aeronautical and Space Sciences

Power output and efficiency of a negative capacitance and inductance shunt for structural vibration control under broadband excitation

Ehtesham Mustafa Qureshi*, Xing Shen and Lulu Chang*****

College of Aerospace Engineering, State Key Laboratory of Mechanics and Control of Mechanical Structures, Nanjing University of Aeronautics and Astronautics, No. 29 Yudao Street, Nanjing 210016, China.

Abstract

Structural vibration control using a piezoelectric shunt is an established control technique. This technique involves connecting a piezoelectric patch, which is bonded onto or embedded into the vibrating structure, to an electric shunt circuit. Thus, vibration energy is converted into electrical energy and is dissipated through a network of electrical components. Different configurations of shunt have been researched, among which the negative capacitance-inductance shunt has gained prominence recently. It is basically an analog, active circuit consisting of operational amplifiers and passive elements to introduce real and imaginary impedance on the vibrating structure. The present study attempts to model the behavior of a negative capacitance-inductance shunt in terms of power output and efficiency using circuit modeling software. The shunt model is validated experimentally and is used to control the structural vibration of an aluminum beam, connected to a pair of piezoelectric patches, under broadband excitation. The model is also used to determine the optimal parameters of a negative capacitance-inductance shunt to increase the efficiency and predict the voltage output limit of op-amp against the supply voltage.

Key words: Piezoelectric, Vibration, Control, Damping, Shunt, Circuit.

1. Introduction

Structural vibration control is important for many reasons, showing prominence in the aerospace field [1-5]. A simple yet effective way of controlling structural vibration is by using piezoelectric patches, either bonded onto or embedded into the vibrating structure, and shunted by an electrical circuit. In piezoelectric shunt damping (PSD), vibration energy is converted into an electrical current and is dissipated through a network of electrical components [6-9]. The direct piezoelectric effect causes the generation of electrical energy in response to the deformation of the piezoelectric patch due to the vibration of the mechanical host structure. On the other hand, in the inverse piezoelectric effect, the piezoelectric patch generates an opposite force on the mechanical vibrating structure when electrical energy is applied to the patch.

The attenuation of structural vibrations requires the accurate design of shunt circuits to counteract the mechanical vibrations and dissipate energy effectively. Forward [7] was the first to propose the idea of using electrical shunt circuits connected to a piezoelectric patch transducer for structural vibration control. An inductive(LC) shunt circuit was used for narrow-band attenuation of resonant mechanical excitation. The inherent capacitive reactance of piezoelectric transducer was cancelled through the inductive shunt for vibration attenuation. Later, Hagood and von Flotow [8] found a correlation between the operation of the LC resonant shunt and a tuned mass damper. They also extended this work to include a resistive element in the existing LC shunt circuit, to make a RLC tuned shunt circuit. Vibration attenuation associated with a particular mode was achieved by adopting an appropriate value of R, and choosing the value of L according to the following equation:

* Ph.D Candidate
** Professor, Corresponding author: shenx@nuaa.edu.cn
*** Ph.D Candidate

Received: January 8, 2015 Revised: March 25, 2015 Accepted: June 11, 2015

http://ijass.org pISSN: 2093-274x eISSN: 2093-2480

$$L = \frac{1}{\omega_i^2 C_p} \quad (1)$$

Here, ω_i is the angular resonant frequency of the *ith* mode of the vibrating structure and C_p is the capacitance of the piezoelectric transducer. The work of Hagood and von Flotow [8] inspired other researchers to address a variety of similar problems. For example, Wu [10] suggested that if a series *RL* shunt is replaced with a parallel shunt, similar damping performance is achieved with the added benefit of performance that is less sensitive to changes in the resistive element. However, the control performance of the resonant shunt is limited to narrow-band vibration attenuation, i.e. at or near the electrical resonance [10-13]. Many different techniques have been used by extending single mode shunts to multiple modes [14-18]. However, the solutions are experimentally difficult to obtain and are also non-adaptive in nature. Therefore, other methods of designing broadband shunts need to be explored.

A simple shunt damping technique, which has shown success in controlling structural vibration over a wide frequency band, is the negative capacitance shunt [19-23,30,31]. Although, inherently, it is a feedback control technique [21], many researchers have used the negative capacitance shunt to cancel the inherent capacitance of the piezoelectric patch in order to increase the power dissipation in the resistive element [19, 24, 25]. The negative capacitive shunt can be synthetically reproduced by using negative impedance circuits. It is basically an active element due to the use of operational amplifiers, which tend to make this shunt unstable if not tuned properly. Previous studies have shown that the negative capacitance in the electrical network artificially increases the electromechancial coupling coefficient of the piezoelectric transducer [7, 26]. This results in a broader frequency range and higher power dissipation. Recently, Beck et al. [27] used a negative capacitance shunt to effectively control the vibration of a flexural system under broadband excitation. The effect of the negative capacitance shunt on the behavior of an electromechanical system consisting of a pair of piezoelectric patches attached to an aluminum beam was studied in detail. The electrical power output of the shunt and the electrical properties of the piezoelectric patch pair were modeled using a circuit modeling software (National Instruments Multisim) and then validated experimentally. A correlation was developed between the power output of the shunt circuit and the amount of vibration suppression, which allowed for better circuit design.

The present study will attempt to extend the studies of Beck et al. [27] by including the effect of inductance in the negative capacitance shunt damping. A synthetic inductor will be used instead of the coil wound inductor in order to conveniently tune the value of inductance and to achieve a high quality factor. According to Eq. (1), in order to damp low frequency vibration, the value of inductance needs to be very large, which is difficult to realize from coil wound inductors. Therefore, a synthetic inductor is used, which is realized with an electronic active circuit comprising operational amplifiers and passive components. The power output and efficiency of a negative capacitance-inductance shunt will be discussed in terms of the change in the shunt parameters to determine how the power output of the circuit affects the control performance of the electromechanical vibration system. First, an analytical model of the negative capacitance-inductance shunt will be developed according to the negative capacitance model presented by Beck et al. [27], which is motivated by control theory. Circuit modeling and experimental analysis is then carried out for both negative capacitance and negative capacitance-inductance shunts. The electrical models will be verified through experiments, depicting their accuracy in predicting the actual results obtained from measurements of negative capacitance and negative capacitance-inductance shunts. A correlation between the output circuit power and the amount of vibration attenuation will also be presented for both the negative capacitance shunt and negative capacitance-inductance shunt circuits, in order to suggest a better circuit design. In order to demonstrate that the proposed negative capacitance-inductance shunt gives better control results than the negative capacitance shunt of Beck et al. [27], an aluminum beam containing a piezoelectric patch pair and shunted by the negative capacitance and negative capacitance-inductance shunt circuits, respectively, will be analyzed experimentally. Next, improvements in the efficiency of the negative capacitance-inductance shunt will be explored by altering the circuit parameters and determining the optimum power output of the operational amplifier (op-amp). Finally, limitations of the op-amp in terms of its output power and supply voltage will be discussed. The paper will then finish with a conclusion.

2. Negative Capacitance-Inductance Shunt

A negative capacitance shunt is basically described by a negative impedance converter as shown in Fig. 1 [28]. It is an active storage element due to the use of an operational amplifier in combination with passive elements. Thus, a particular negative impedance can be produced by varying the values of Z_3 and Z_4. The circuit's input impedance can be

DOI: http://dx.doi.org/10.5139/IJASS.2015.16.2.223

written as:

$$Z_n = -\frac{Z_3 Z_2}{Z_4} \tag{2}$$

and the impedance of the *ith* circuit element is:

$$Z_n = R_i + i\omega L_i + \frac{1}{i\omega C_i} \tag{3}$$

The negative capacitance circuit as shown in Fig. 2 will be used in this study. Its input impedance is given by:

$$Z_n = -\frac{R_3}{R_4}\left[\frac{(R_2)(1/i\omega C_2)}{R_2 + 1/i\omega C_2}\right] \tag{4}$$

The resistor R_2 is important for the stability of the op-amp at DC, but as its size is large, it can be taken as negligible [27]. Therefore, Eq. (4) can be simplified to:

$$1/i\omega C_n = -\frac{R_3}{R_4} 1/i\omega C_2 \tag{5}$$

Thus, the negative capacitance value after rearranging the above equation is:

$$C_n = -\frac{R_4}{R_3} C_2 \tag{6}$$

where C_2 is the reference capacitor.

As mentioned in Section 1, a synthetic inductor is used in this work instead of a coil wound physical inductor. This is because the coil wound inductors could be of large size, requiring high inductance values for low frequency vibration control according to Eq. (1), which is difficult to realize practically, especially for low frequency aerospace applications, where weight could have a negative effect on the performance and efficiency. Also, reducing the size of the coil inductor reduces inductance and the quality factor. The synthetic inductor used in this study is based on Riordan-type inductor [29] and is shown in Fig. 3. The input impedance Z_{Ls} of the circuit is equivalent to:

$$Z_{L_s} = s\frac{R_{10}R_{11}C_i}{R_{12}}R_{13} \tag{7}$$

The equivalent inductance of the synthetic circuit L_s=$R_{10}R_{11}C_iR_{13}/R_{12}$, where R_{13} is the adjustable resistance for inductance tuning. By carefully selecting the impedance values of the circuit elements of the synthetic inductor, the electrical quality factor Q_i can be adjusted in a certain range.

Figure 4 shows the complete negative capacitance-inductance shunt, which includes a negative capacitor, a resistor, and an inductor in series with the electrical model of a piezoelectric patch. The electrical model of a piezoelectric patch is represented by a capacitor and a strain-induced voltage source. The magnitude of the voltage source is strongly dependent on the amount of strain produced by the vibrating structure on which this piezoelectric patch is

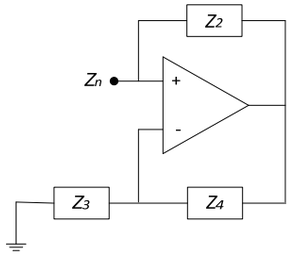

Fig. 1. Schematic diagram of a negative impedance converter.

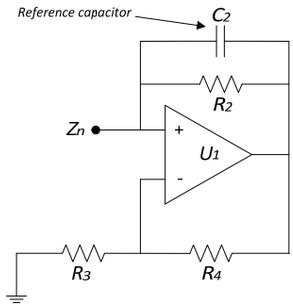

Fig. 2. Schematic representation of a negative capacitance circuit.

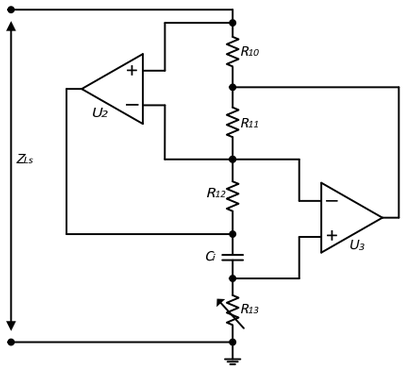

Fig. 3. Riordan's simulated grounded inductor.

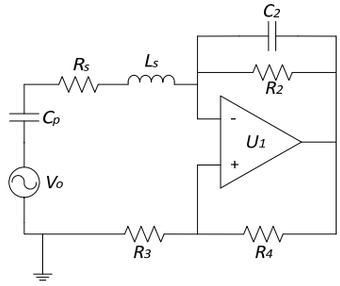

Fig. 4. Complete schematic diagram of negative capacitance-inductance shunt attached to a piezoelectric patch.

attached. Therefore, this value will be strongly dependent on frequency for a particular system [27].

The total impedance of negative capacitance-inductance shunt shown in Fig. 4 is:

$$Z_{sh} = R_s + i\omega L_s + {}^{1}/_{i\omega C_n} \tag{8}$$

To validate the numerical circuit with the experiment, the negative capacitance circuit is constructed by using an OPA445AP operational amplifier. The negative capacitance value is varied by changing the potentiometer value for the resistance ratio R_4/R_3 according to Eq. (6). The series resistor R_s is also a potentiometer for straightforward and continuous adjustment. On the other hand, the series inductor L_s is constructed by using two OPA445AP operational amplifiers along with four resistances as shown in Fig. 3. The inductance value is varied by changing the potentiometer value for the resistance R_{13} according to Eq. (7).

The circuit shown in Fig. (4) also leads to the calculation of shunt power. Since the piezoelectric patch, negative capacitor, series resistor, and inductor are all in series, the current within the circuit can be calculated as:

$$I_{sh} = \frac{V_o}{(i\omega C_p)^{-1}+Z_{sh}} \tag{9}$$

and the voltage across the shunt circuit is:

$$V_{sh} = I_{sh} Z_{sh} \tag{10}$$

Therefore, the shunt power is given by:

$$S_{shunt} = {V_o}^2 \frac{Z_{sh}}{[(i\omega C_p)^{-1}+Z_{sh}]^2} \tag{11}$$

This equation is similar to that in Beck et al. [27], with the exception that the additional effect of a series synthetic inductor has been considered here in the shunt impedance Z_{sh}.

3. Numerical Modeling of Negative Capacitance-Inductance Shunt Circuit

The circuit model is designed in National Instruments Multisim as shown in Fig. 5, in accordance with the scheme used by Beck et al. [27]. This model consists of a piezoelectric patch connected in series to a negative capacitance-inductance shunt. The piezoelectric patch is modeled using its electrical equivalent model, which is comprised of a capacitor C_p and strain-induced voltage V_1.

This model includes all the components necessary for experimental implementation. A manufacturer provided electrical model of op-amp is also included to accurately simulate its electrical behavior. The impedances of two voltage probes, V_2 and V_3, are also added to the circuit in order to accurately compare the experimental and simulated circuit response. The voltage probe V_2 is used to determine the output current of op-amp U_1 by measuring the voltage

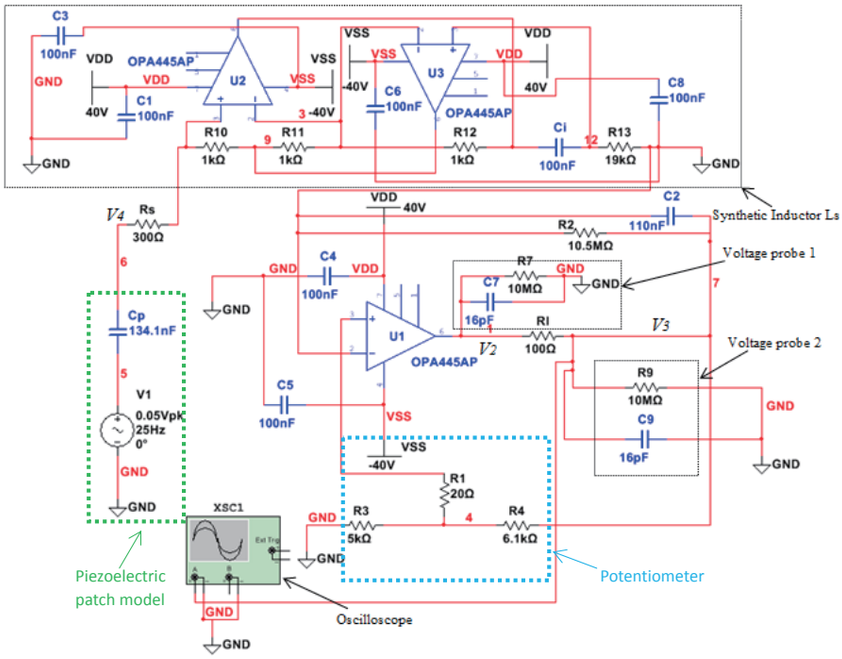

Fig. 5. Negative capacitance-inductance shunt and piezoelectric patch circuit model.

DOI: http://dx.doi.org/10.5139/IJASS.2015.16.2.223

drop across the small resistor R_t. On the other hand, voltage probe V_3 is used to measure the output voltage of op-amp U_1, which is consistent with the probe used in experiments. The temporal response of the model is measured by a virtual oscilloscope, while the frequency response of the model is obtained by using the AC circuit analyzer included in the Multisim software.

The impedance of the circuit model is found by dividing the voltage V_3 by the current through the series resistance R_s, i.e.:

$$Z_{sim} = \frac{V_3}{I_{R_S}} \tag{12}$$

where Z_{sim} represents the simulated impedance.

Beck et al. [27] defined the efficiency of the negative capacitive shunt as:

$$\eta = \frac{S_{shunt}}{S_{op-amp}} \tag{13}$$

where S_{shunt} is the power output of the shunt and $S_{op\text{-}amp}$ is the power supplied by the op-amp U_1. This equation (13) will also be used here to investigate the change in efficiency of the negative capacitance-inductance shunt for control of structural vibration under broadband excitation. The power output of the shunt can be calculated by:

$$S_{shunt} = V_4 I_{R_S} \tag{14}$$

Here, V_4 is the total voltage across the full shunt circuit and I_{Rs} is the current through the series resistor R_s, as shown in Fig.5.

4. Experimental Setup and Control Scheme

To verify the electrical model as shown in Fig. 5, experiments were performed on a cantilever aluminum beam with a pair of piezoelectric patches attached. Fig. 6 shows all the necessary equipment, their configuration and experimental setup, while Table 1 lists the beam and piezoelectric patch properties and dimensions. A Tektronix function generator is used to give a short sine sweep signal in order to excite the frequency range of interest. A frequency range of 1 to 500 Hz is selected according to the piezostructural configuration, with the first four frequency modes lying in this frequency range. This enabled us to properly identify the frequency modes using FFT analysis in order to investigate the control performance of the shunt circuit under different parameters; this will be discussed in the next section. The piezostructure is subjected to base excitation, as is usually the case in many aerospace structures. The tip response of the cantilever beam is measured by an Optex FA laser sensor. This information is then fed into the computer with a National Instruments PCIe-7842R RIO device for signal processing using Labview software. The piezoelectric patch pair is connected to the shunt circuit and its response is analyzed for different circuit parameters under broadband excitation.

To measure the electrical behavior of the shunt circuit during the control of a cantilever beam, the method as

Table 1. Aluminum beam and piezoelectric patch properties and dimensions.

Aluminum beam	Size	300 x 40 x 1 mm
	Elastic modulus	E_b = 70 GPa
	Mass density	ρ_b = 2700 kg/m^3
Piezoelectric patch	Size	50 x 40 x 0.5 mm
	Elastic modulus	E_p = 66 GPa
	Mass density	ρ_p = 7450 kg/m^3
	Electromechanical coupling coefficient	k_{31} = 0.36
	Total capacitance	C_p = 134.1 nF

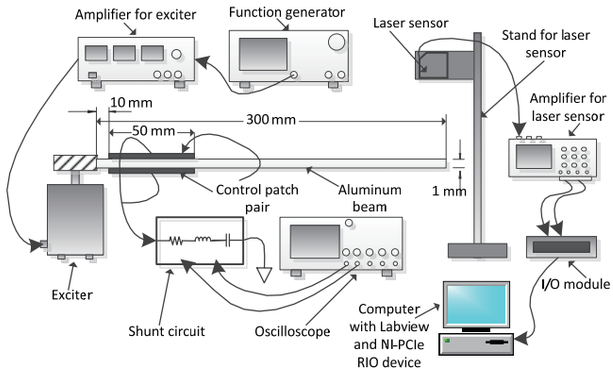

Fig. 6. Experimental setup.

outlined by Beck et al. [27] will be used here and is described again for convenience. In this method, the key parameter of interest is the power output of the operational amplifier. Fig. 7 shows the full negative capacitance-inductance shunt circuit with measurement probe locations used for experimental validation. The output voltage of op-amp U_1 is measured using a voltage probe at location V_3, while the current is measured by determining the voltage drop over a small resistor R_I placed at the output pin of the op-amp U_1. The complex power output of op-amp U_1 is given by:

$$S = [\bar{V}_3 I] \tag{15}$$

where the current is:

$$I = \frac{V_I}{R_I} \tag{16}$$

and the voltage drop across the resistor R_I is:

$$V_I = V_2 - V_3 \tag{17}$$

The complex power can be expressed as:

$$S = P + i\,Q \tag{18}$$

where P is the real power and Q is the reactive power, while the apparent power is the magnitude of the complex power, i.e. |S|.

5. Results and Discussion

5.1 Model Verification Through Experimentation

For verification of the model, the procedure as described by Beck et al. [27] is followed to measure the power output of op-amp U_1, both numerically and experimentally, for the full negative capacitance shunt (Fig. 7 excluding L_s) and full negative capacitance-inductance shunt (Fig. 7). For this purpose, four values of series resistance R_s, three values of series inductance L_s, and three values of negative capacitance C_n were used. Table 2 shows the circuit parameters used for simulations and experiments.

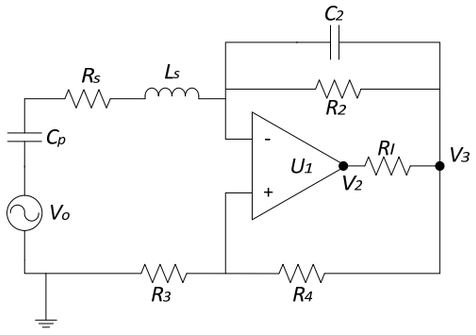

Fig. 7. Complete schematic diagram of negative capacitance-inductance shunt circuit with measurement probe locations V_2 and V_3.

5.1.1 Full Negative Capacitance Shunt

Simulations and experiments were performed for the full negative capacitance shunt to measure the power output of op-amp U_1, for four different values of series resistance R_s at constant negative capacitance C_n=-134.23, as shown in Figs. 8 and 9, respectively. Both the model solution and the experimental measurement of power are normalized with respect to the power of the piezoelectric patch in the absence of any shunt attached, as suggested by Beck et al. [27]. Eq. (19) gives the power of the piezoelectric patch when no shunt is attached, i.e.

$$S_p = \frac{V_o^2}{i\omega C_p} \tag{19}$$

where V_o and C_p represent the strain induced voltage and the capacitance of the piezoelectric patch, respectively. A comparison of Figs. 8 and 9 shows almost exact matching of both the normalized output power magnitude and phase plots, which verified the full negative capacitance model with the experiments. These Figures are obtained by using a negative capacitor of -134.23 nF for all the four resistors. Few small peaks are observed in the experimental phase plot of Fig. 9 at higher frequencies, which may be due to the higher order harmonics of the first resonance mode. A close examination of Figs. 8 and 9 suggests that at very low

Table 2. Circuit parameters for simulations and experiments.

V_o	0.05 V
C_p	134.1 nF
C_2	110 nF
R_2	10.5 MΩ
R_3	5.0 kΩ
R_4	6.1 kΩ
C_i	100 nF
R_{10}	1.0 kΩ
R_{11}	1.0 kΩ
R_{12}	1.0 kΩ
R_{13}	19.0 kΩ

DOI: http://dx.doi.org/10.5139/IJASS.2015.16.2.223

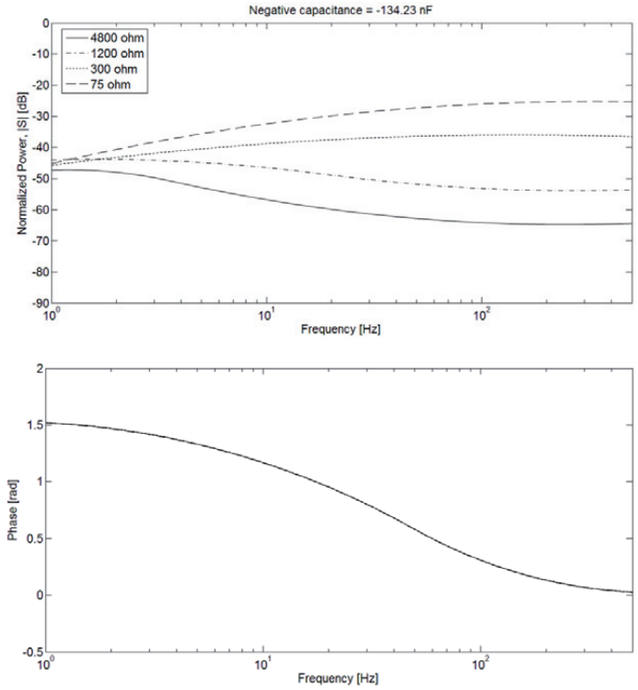

Fig. 8. Simulated normalized power output of the op-amp, amplitude and phase, for four values of series resistance R_s for full negative capacitance shunt.

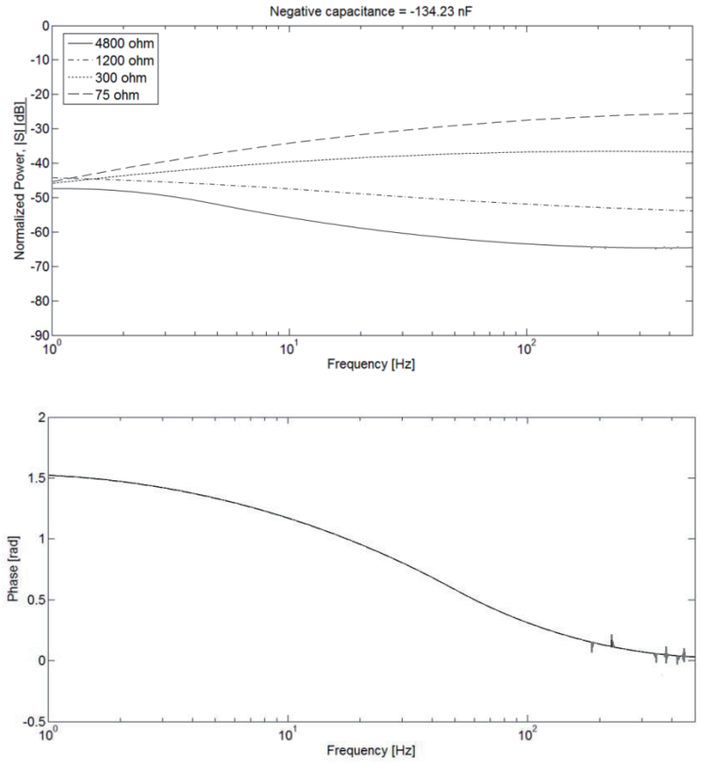

Fig. 9. Experimental normalized power output of the op-amp, amplitude and phase, for four values of series resistance R_s for full negative capacitance shunt.

frequencies, i.e. < 2 Hz, the power output of op-amp for all the four resistances is similar. For higher frequencies, 75 ohm and 300 ohm resistances showed an increase in the output power, while the 1200 ohm and 4800 ohm resistances showed a decrease in the output power. After approximately 100 Hz, the power output for all the resistances is stable and constant. Similar to the results of Beck et al. [27], the phase of power is not changed for different resistance values, which indicates that the series resistor only affects the bandwidth of the gain of negative capacitance shunt and does not affect its impedance.

Figure 10 presents the tip response of the aluminum cantilever beam for the four values of series resistance R_s of the negative capacitance shunt along with the uncontrolled response. The first four resonance frequencies are clearly visible in the frequency range of interest. Few small peaks are observed at higher frequencies, which may be due to the higher order harmonics of the first resonance mode. From Fig. 10 it is clear that series resistance R_s affects the amount of vibration suppression at different resonance modes. For the first resonance mode around 10 Hz, the 300 ohm resistor results in the greatest attenuation, while the 75 ohm resistor performed better than other resistors for higher modes. It should be noted that a certain level of power output does not necessarily correlate to more control, especially at low frequencies. This may be observed from the examination of Figs. 8, 9, and 10 for the first resonance frequency at around 10 Hz. In Figs. 8 and 9, the 75 ohm resistor results in the highest output power, while the amount of vibration suppression achieved from this resistor is lower than the 300 ohm resistor, as shown in Fig. 10. The control performance in terms of the displacement magnitude (dB) of full the negative capacitance shunt for four values of series resistance R_s is shown in Table 3. The total apparent power output of op-amp for the four values of series resistor R_s is shown in Table 4. From Table

Table 4. Total apparent (VA) power of op-amp for four values of series resistance R_s from 1 to 500 Hz for full negative capacitance shunt.

R_s = 4800 ohm	R_s = 1200 ohm	R_s = 300 ohm	R_s = 75 ohm
0.005	0.032	0.174	0.843

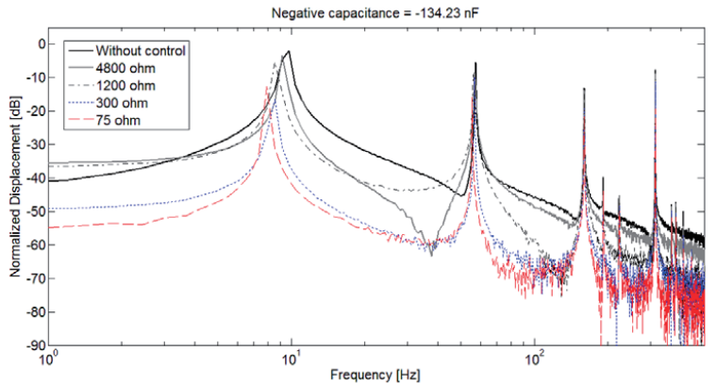

Fig. 10. Tip response of the cantilever beam for four values of series resistance R_s for full negative capacitance shunt.

Table 3. Control performance in terms of displacement magnitude (dB) of full negative capacitance shunt for four values of series resistance R_s.

	First mode, Peak value (upper) and reduction (lower)	Second mode, Peak value (upper) and reduction (lower)	Third mode, Peak value (upper) and reduction (lower)	Fourth mode, Peak value (upper) and reduction (lower)
Without control	-2.02	-5.56	-13.10	-7.75
	-	-	-	-
4800 ohm	-3.35	-8.43	-13.76	-8.81
	1.33	2.87	0.66	1.06
1200 ohm	-5.27	-9.05	-14.87	-10.55
	3.25	3.49	1.77	2.80
300 ohm	-16.25	-9.75	-19.21	-11.31
	14.23	4.19	6.11	3.56
75 ohm	-12.80	-15.81	-21.39	-19.28
	10.78	10.25	8.29	11.53

DOI: http://dx.doi.org/10.5139/IJASS.2015.16.2.223

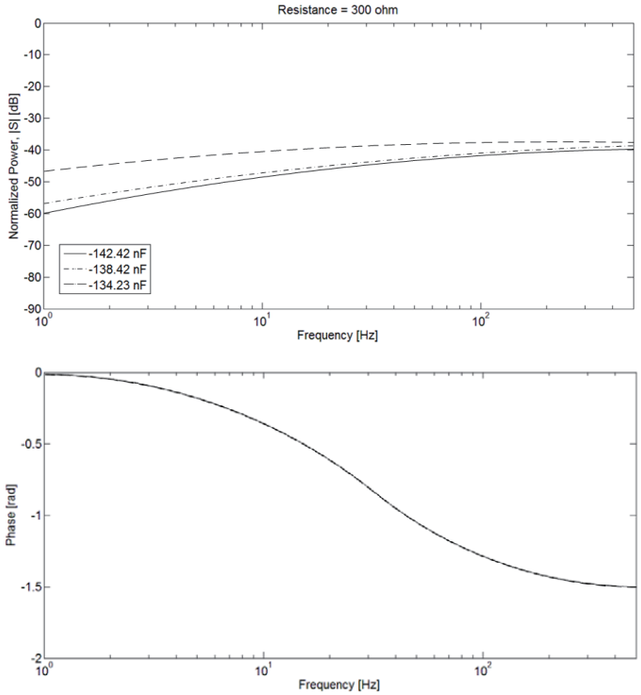

Fig. 11. Simulated normalized power output of the op-amp, amplitude and phase, for three values of negative capacitance C_n for full negative capacitance shunt.

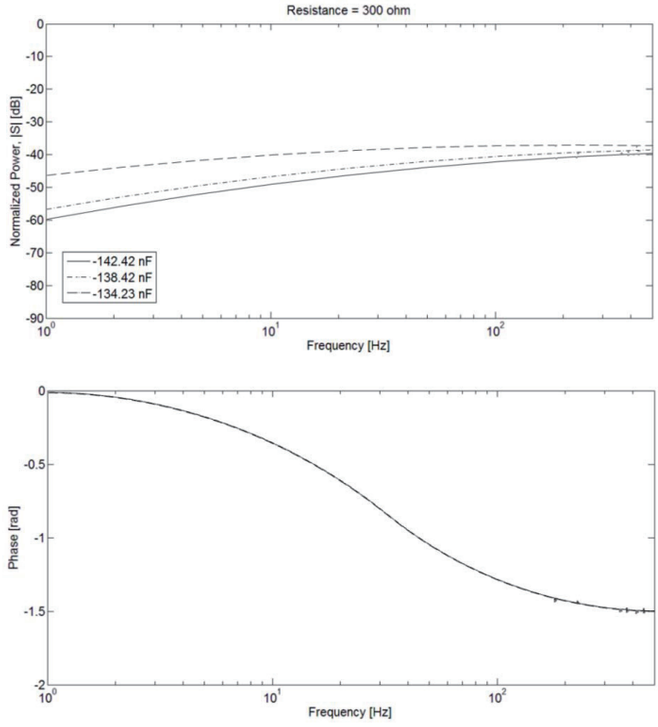

Fig. 12. Experimental normalized power output of the op-amp, amplitude and phase, for three values of negative capacitance C_n for full negative capacitance shunt.

4, it is clear that the total apparent power increases as the series resistance R_s decreases. Also, the overall response of the beam decreases with the increase in the apparent power for broadband vibration control. Therefore, to achieve more vibration suppression, it is necessary to increase the apparent power output of op-amp for the frequency range of interest.

Figures 11 and 12 show the normalized power output and phase plots of op-amp U_1 for three values of negative capacitance and constant series resistance of 300 ohm. Again, the simulated and experimental plots are equivalent, which verifies the full negative capacitance shunt model with the experiment. A comparison of Figs. 11 and 12 with Figs. 8 and 9 suggests that, in contrast to changing the resistance values, changing the negative capacitance values has a greater effect on the output power magnitude of op-amp at low frequencies, while for higher frequencies, this change has little effect. Similar to the resistance case of Figs. 8 and 9, the phase of the power remains the same for different negative capacitance values. The tip response of the beam is shown in Fig. 13, which shows that vibration suppression increases with the decrease in the negative capacitance values. Table 5 shows the control performance in terms of displacement magnitude (dB) of the full negative capacitance shunt for three values of negative capacitance. A comparison of Figs. 11 and 12 with Fig. 13 suggests that the vibration suppression from Fig. 13 does not follow the trend observed in Figs. 11 and 12. That is, at low frequencies, the power output is less than that of the higher frequencies, while Fig. 13 suggests that vibration suppression is greater at low frequencies than at high frequencies. This again demonstrates that a certain level of power output does not necessarily correlate to greater control. The total apparent power output of op-amp for three values of negative capacitance is shown in Table 6. This Table shows that the negative capacitance value which is near to the piezoelectric patch capacitance has the greatest total apparent power output of op-amp. Increasing the negative capacitance value to greater than this value decreases the total apparent power output of op-amp.

Table 6. Total apparent (VA) power of op-amp for three values of negative capacitance C_n from 1 to 500 Hz for full negative capacitance shunt.

C_n = -142.42 nF	C_n = -138.42 nF	C_n = -134.23 nF
0.136	0.152	0.174

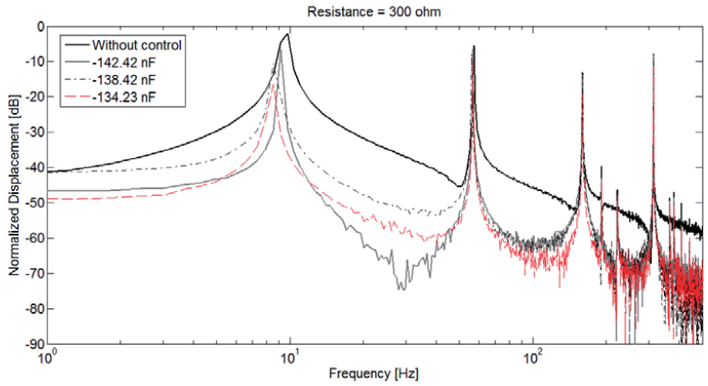

Fig. 13. Tip response of the cantilever beam for three values of negative capacitance C_n for full negative capacitance shunt.

Table 5. Control performance in terms of displacement magnitude (dB) of full negative capacitance shunt for three values of negative capacitance C_n.

	First mode, Peak value (upper) and reduction (lower)	Second mode, Peak value (upper) and reduction (lower)	Third mode, Peak value (upper) and reduction (lower)	Fourth mode, Peak value (upper) and reduction (lower)
Without control	-2.02	-5.56	-13.10	-7.75
	-	-	-	-
-142.42 nF	-6.64	-6.65	-13.57	-8.21
	4.62	1.09	0.47	0.46
-138.42 nF	-10.62	-7.82	-14.15	-8.81
	8.60	2.26	1.41	1.06
-134.23 nF	-16.25	-9.75	-19.21	-11.31
	14.23	4.19	6.11	3.56

DOI: http://dx.doi.org/10.5139/IJASS.2015.16.2.223

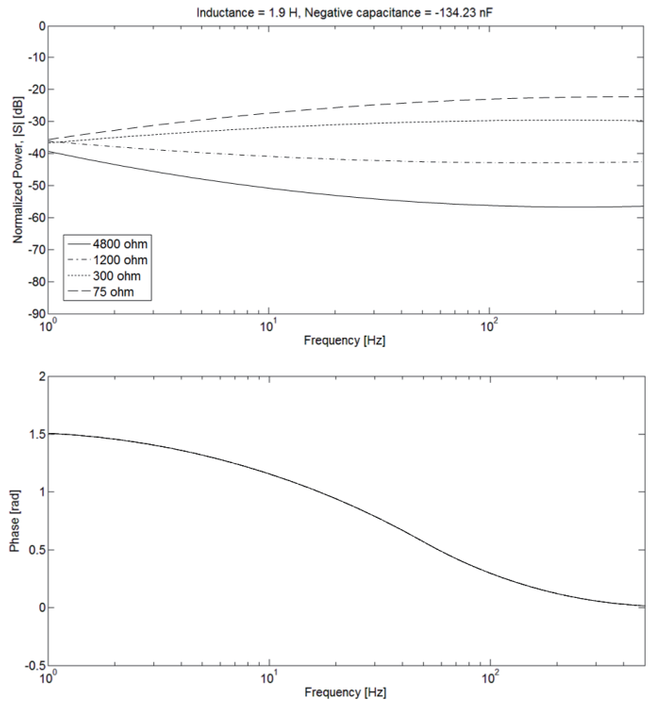

Fig. 14. Simulated normalized power output of the op-amp, amplitude and phase, for four values of series resistance R_s for full negative capacitance-inductance shunt.

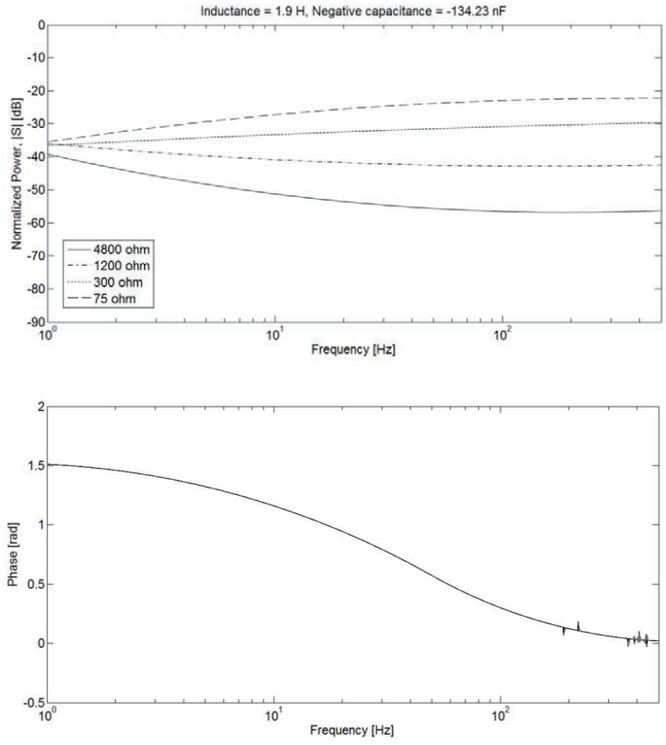

Fig. 15. Experimental normalized power output of the op-amp, amplitude and phase, for four values of series resistance R_s for full negative capacitance-inductance shunt.

From the above discussion, it is clear that the series resistor works best for high frequency vibration control, while the negative capacitance gives better results for low frequency vibration suppression. Thus, in conclusion it can be said that if a negative capacitance shunt circuit is to be used for the control of broadband vibration, a circuit model needs to be used to select the appropriate circuit parameters for best damping performance.

5.1.2 Full Negative Capacitance-Inductance Shunt

The normalized simulated and experimental output power and phase plots of op-amp U_1 for four values of series resistance R_s at constant negative capacitance C_n=-134.23 and inductance L_s=1.90 H are shown in Figs. 14 and 15, respectively. Figs. 14 and 15 are similar, which verified the shunt model with the experiments for the full negative capacitance-inductance shunt. The tip response of the beam for the four values of series resistance is shown is Fig. 16. An examination of Figs. 14, 15, and 16 indicates similar trends as shown in Figs. 8, 9, and 10 respectively. In other words, the 300 ohm resistor has the greatest suppression for the first resonance mode, while the 75 ohm resistor performed better than the other resistors for the remaining modes in the frequency range of interest. This is also clear from Table 7, which shows the control performance in terms of the displacement magnitude (dB) of the full negative capacitance-inductance shunt for the four values of series resistance. An examination of the first resonance mode near 10 Hz from Figs. 14, 15, and 16 suggests that the 300 ohm resistor has the greatest suppression at this frequency, while the corresponding power output of op-amp is lower than that from the 75 ohm resistor. This supports the earlier argument that greater power output of op-amp does not necessarily mean greater vibration suppression at that particular frequency. The total apparent power output of op-amp for the four values of series resistor R_s is shown in Table 8. This table shows that the total apparent power output decreases with the increase in resistor value i.e. the 4800 ohm has the least apparent power output while the 75 ohm has the highest. This trend is similar to that witnessed

Table 7. Control performance in terms of displacement magnitude (dB) of full negative capacitance-inductance shunt for four values of series resistance R_s.

	First mode, Peak value (upper) and reduction (lower)	Second mode, Peak value (upper) and reduction (lower)	Third mode, Peak value (upper) and reduction (lower)	Fourth mode, Peak value (upper) and reduction (lower)
Without control	-2.02	-5.56	-13.10	-7.75
	-	-	-	-
4800 ohm	-3.71	-10.05	-14.32	-9.72
	1.69	4.49	1.22	1.97
1200 ohm	-6.65	-10.58	-15.35	-11.31
	4.63	5.02	2.25	3.56
300 ohm	-21.74	-14.90	-16.31	-15.75
	19.72	9.34	3.21	8.0
75 ohm	-16.89	-17.44	-22.33	-22.99
	14.87	11.88	9.23	15.24

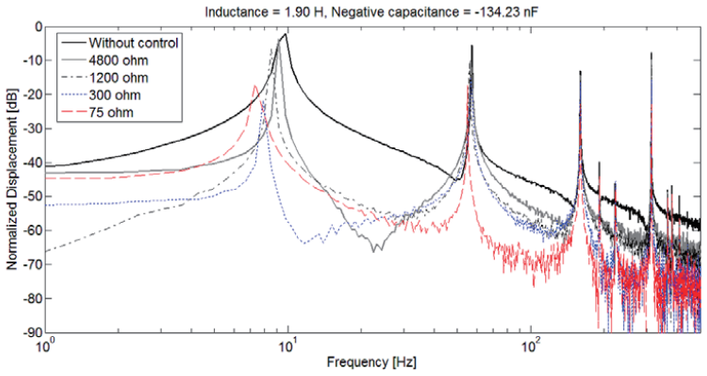

Fig. 16. Tip response of the cantilever beam for four values of series resistance R_s for full negative capacitance-inductance shunt.

DOI: http://dx.doi.org/10.5139/IJASS.2015.16.2.223

for the full negative capacitance shunt. The phase plots of the output power are the same for all the resistor values, which indicates that the series resistor only affects the bandwidth of the gain of the negative capacitance-inductance shunt circuit, but does not affect its impedance.

Figures 17 and 18 show the simulated and experimental normalized power output of op-amp U_1, respectively, for three negative capacitance values at constant resistance R_s=300 ohm and inductance L_s=1.90 H. These two plots are similar, which verifies the full negative capacitance-inductance shunt model with the experiment. Again, the phase of the power is not affected by the negative capacitance. A comparison of Figs. 17 and 18 with Figs. 14 and 15 suggests that in contrast to changing the resistance values, changing the negative capacitance values has a greater effect on the output power magnitude of op-amp at low frequencies, while for the higher frequencies, this change has little effect. This was also observed for the case of the full negative capacitance shunt. Similar to the resistance cases of Figs. 14 and 15, the phase of the power remains the same for different negative capacitance values. The tip response of the beam is shown in Fig. 19, which shows that vibration suppression increases with the decrease in the negative capacitance values. Table 9 shows the control performance in terms of the displacement magnitude (dB) of the full negative capacitance-inductance shunt for three values of negative capacitance. A comparison of Figs. 17 and 18 with Fig. 19 suggest that the vibration suppression from Fig. 19 does not follow the trend observed in Figs. 17 and 18. That is, at low frequencies, the power output is less than that at the higher frequencies, while Fig. 19 suggests that vibration suppression is greater at low frequencies than at high frequencies. This again reveals that a certain level of power output does not necessarily correlate to greater control. The total apparent power output of op-amp for three values of negative capacitance is shown in

Table 8. Total apparent (VA) power of op-amp for four values of series resistance R_s from 1 to 500 Hz for full negative capacitance-inductance shunt.

R_s = 4800 ohm	R_s = 1200 ohm	R_s = 300 ohm	R_s = 75 ohm
0.013	0.052	0.372	1.483

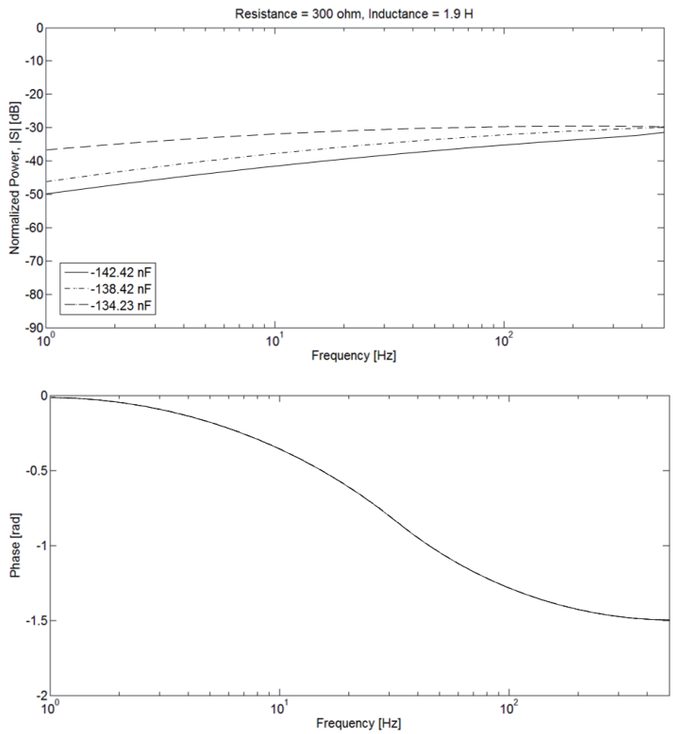

Fig. 17. Simulated normalized power output of the op-amp, amplitude and phase, for three values of negative capacitance C_n for full negative capacitance-inductance shunt.

Table 10. This Table shows that the negative capacitance value, which is close to the piezoelectric patch capacitance, has the greatest total apparent power output of op-amp. Increasing the negative capacitance value to greater than this value decreases the total apparent power output of op-amp.

Figures 20 and 21 show the simulated and experimental normalized power output, respectively, of op-amp U_1 for three series inductance values at constant resistance R_s=300 ohm and negative capacitance C_n=-134.23. These two plots are similar, which verifies the full negative capacitance-inductance shunt model with the experiment. Again, the phase of the power is not affected by the series

Table 10. Total apparent (VA) power of op-amp for three values of negative capacitance C_n from 1 to 500 Hz for full negative capacitance-inductance shunt.

C_n = -142.42 nF	C_n = -138.42 nF	C_n = -134.23 nF
0.284	0.307	0.372

Table 9. Control performance in terms of displacement magnitude (dB) of full negative capacitance-inductance shunt for three values of negative capacitance C_n.

	First mode, Peak value (upper) and reduction (lower)	Second mode, Peak value (upper) and reduction (lower)	Third mode, Peak value (upper) and reduction (lower)	Fourth mode, Peak value (upper) and reduction (lower)
Without control	-2.02	-5.56	-13.10	-7.75
	-	-	-	-
-142.42 nF	-12.20	-10.10	-13.76	-8.81
	10.18	4.54	0.66	1.06
-138.42 nF	-15.94	-10.59	-14.35	-9.72
	13.92	5.03	1.25	1.97
-134.23 nF	-21.74	-14.90	-16.31	-15.75
	19.72	9.34	3.21	8.0

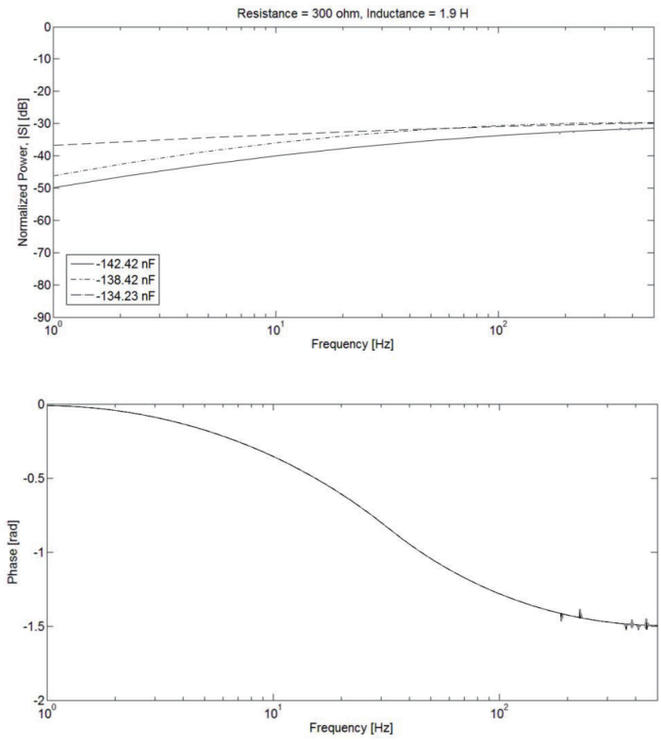

Fig. 18. Experimental normalized power output of the op-amp, amplitude and phase, for three values of negative capacitance C_n for full negative capacitance-inductance shunt.

DOI: http://dx.doi.org/10.5139/IJASS.2015.16.2.223

inductance. The examination of Figs. 20 and 21 indicates that the difference between output power of op-amp for the three series inductance values is much larger, especially for very low frequencies, than that observed for the series resistances in Figs. 14 and 15 and negative capacitances in Figs. 17 and 18. Also, the power output for an inductance of 1.90 H is much larger than that of the other two inductances, i.e. 0.66 H and 1.08 H, which remain close to each other throughout the frequency range of interest. The much higher power output for an inductance of 1.90 H for very low frequencies is attributed to the high inductance value as compared to the other two inductance values of 0.66 H and 1.08 H, respectively. The tip response of a beam is shown in Fig. 22, which indicates that the vibration suppression increases with the increase in the inductance values, especially for low frequencies. This is also verified from Eq. (1), which indicates that for low frequency vibration suppression, the value of inductance needs to be high. As mentioned previously, a certain level of power output does not necessarily correlate to more

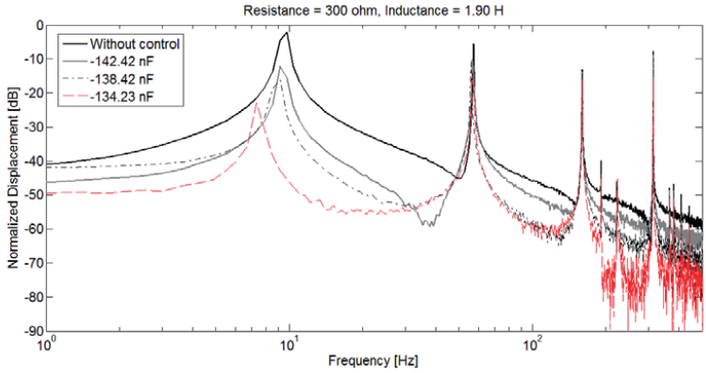

Fig. 19. Tip response of the cantilever beam for three values of negative capacitance C_n for full negative capacitance-inductance shunt.

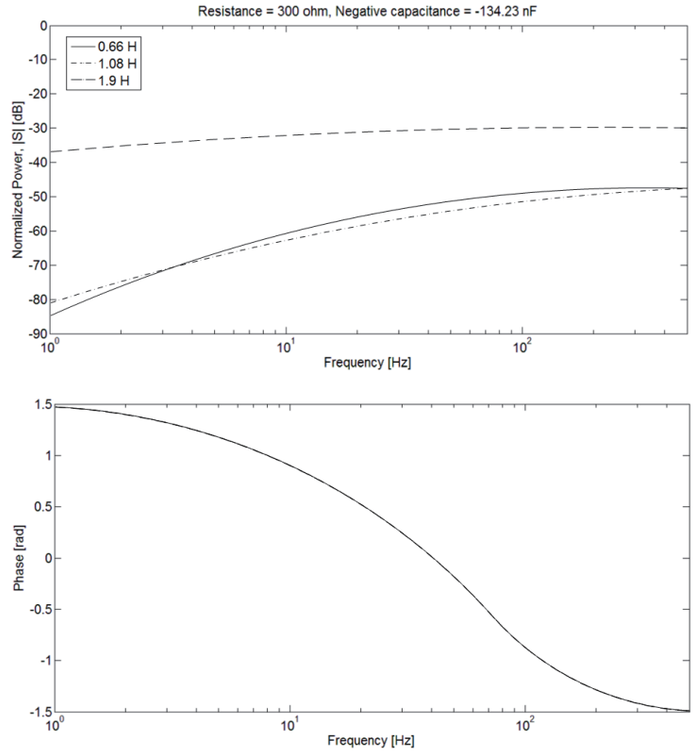

Fig. 20. Simulated normalized power output of the op-amp, amplitude and phase, for three values of series inductance L_s for full negative capacitance-inductance shunt.

control. This argument is verified from the examination of Fig. 21, which indicates that the output power of op-amp for the inductances of 0.66 H and 1.08 is exactly the same at the frequency of 4 Hz, while the control performance of 1.08 H is better than 0.66 H at the same frequency (see Fig. 22). Table 11 shows the control performance in terms of the displacement magnitude (dB) of the full negative capacitance-inductance shunt for three values of series inductance. The total apparent power output of op-amp for the three values of series inductance is shown in Table 12. This table shows that the total apparent power output increases with the increase in inductor value, i.e. the 1.90 H inductor has the highest apparent power output followed

Table 12. Total apparent (VA) power of op-amp for three values of series inductance L_s from 1 to 500 Hz for full negative capacitance-inductance shunt.

L_s = 1.90 H	L_s = 1.08 H	L_s = 0.66 H
0.372	0.108	0.092

Table 11. Control performance in terms of displacement magnitude (dB) of full negative capacitance-inductance shunt for three values of series inductance L_s.

	First mode, Peak value (upper) and reduction (lower)	Second mode, Peak value (upper) and reduction (lower)	Third mode, Peak value (upper) and reduction (lower)	Fourth mode, Peak value (upper) and reduction (lower)
Without control	-2.02	-5.56	-13.10	-7.75
	-	-	-	-
1.90 H	-21.74	-14.90	-16.31	-15.75
	19.72	9.34	3.21	8.0
1.08 H	-4.66	-10.38	-13.84	-8.81
	2.64	4.82	0.74	1.06
0.66 H	-3.07	-7.97	-13.40	-8.21
	1.05	2.41	0.30	0.46

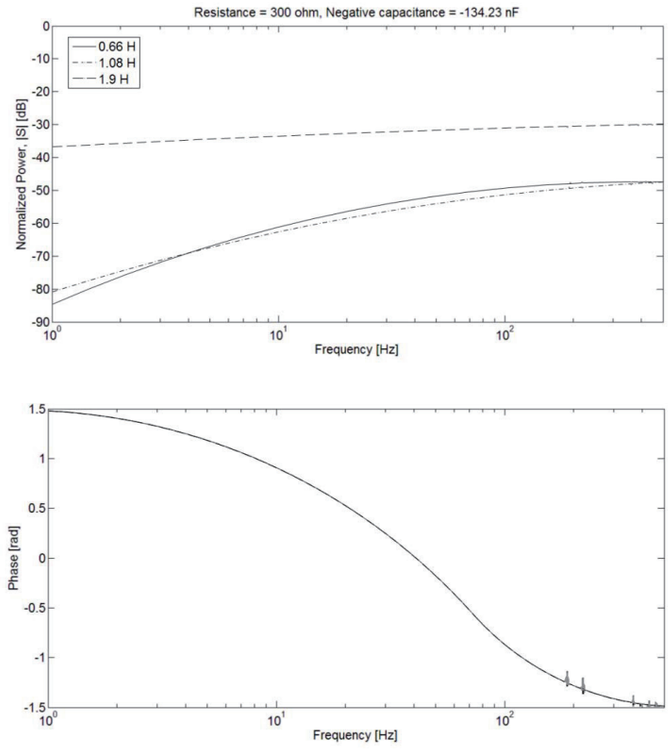

Fig. 21. Experimental normalized power output of the op-amp, amplitude and phase, for three values of series inductance L_s for full negative capacitance-inductance shunt.

DOI: http://dx.doi.org/10.5139/IJASS.2015.16.2.223

by the 1.08 H and 0.66 H inductors. Also, the difference in the total apparent power output between the 0.66 H and 1.08 H inductors is not significant; this is because low frequency vibration attenuation requires high inductance values as is shown in Eq. (1).

5.1.3 Full Negative Capacitance vs. Full Negative Capacitance-Inductance Shunt

In order to demonstrate the better vibration control performance of the proposed shunt, the tip response of the beam is obtained for the full negative capacitance shunt and full negative capacitance-inductance shunt circuits as shown in Fig. 23. Table 13 indicates the control performance in terms of the displacement magnitude (dB) of full negative capacitance and the full negative capacitance-inductance shunt. Both Fig. 23 and Table 13 clearly indicate better vibration attenuation of the beam using the full negative capacitance-inductance shunt compared to using

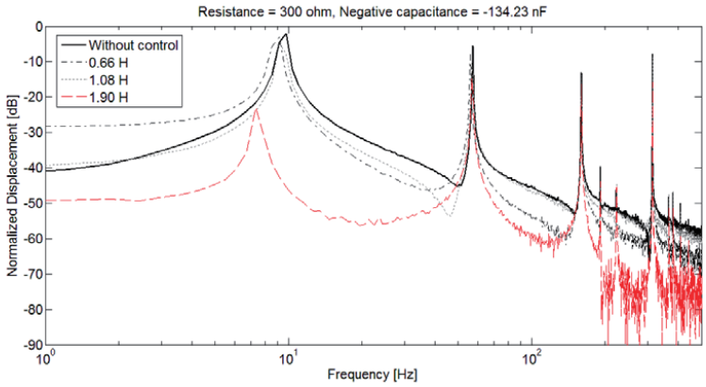

Fig. 22. Tip response of the cantilever beam for three values of series inductance L_s for full negative capacitance-inductance shunt.

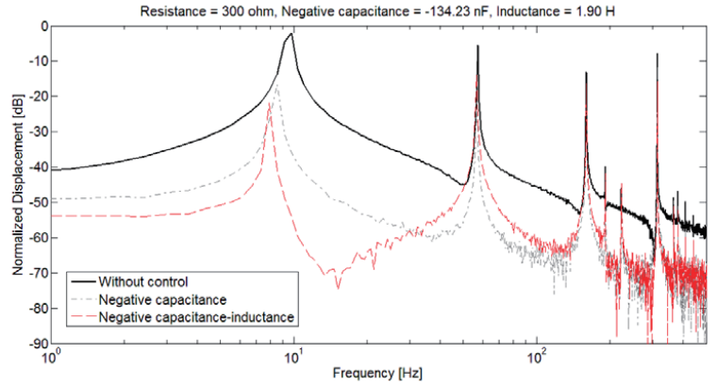

Fig. 23. Tip response of the cantilever beam for full negative capacitance shunt vs full negative capacitance-inductance shunt.

Table 13. Control performance in terms of displacement magnitude (dB) of full negative capacitance vs full negative capacitance-inductance shunt.

	First mode, Peak value (upper) and reduction (lower)	Second mode, Peak value (upper) and reduction (lower)	Third mode, Peak value (upper) and reduction (lower)	Fourth mode, Peak value (upper) and reduction (lower)
Without control	-2.02	-5.56	-13.10	-7.75
	-	-	-	-
Negative capacitance	-16.25	-9.75	-19.21	-11.31
	14.23	4.19	6.11	3.56
Negative capacitance-inductance	-21.74	-14.90	-16.31	-15.75
	19.72	9.34	3.21	8.0

the full negative capacitance shunt. Although the vibration attenuation obtained from the negative capacitance shunt is larger than that obtained from the negative capacitance-inductance shunt for the third resonant mode, the overall performance of the negative capacitance-inductance shunt is still considerably superior to the negative capacitance shunt for the control of the beam under broadband excitation.

It is also important to note that for the full negative capacitance shunt circuit, in order to reduce the first resonant mode by 14.23 dB, the change of resistor values from 4800 ohm to 75 ohm requires more power than that required by the change of negative capacitance values from -142.42 nF to -134.23 nF, as is apparent from Tables 4 and 6, respectively. Thus, in order to achieve low frequency vibration suppression, it is suggested that the negative capacitor values are changed instead of the series resistor values, which are more effective for high frequency vibration control.

For the full negative capacitance-inductance shunt circuit, in order to reduce the first resonant mode by 19.72 dB, the change of resistor values from 4800 ohm to 75 ohm require more power followed by the change of inductor from 1.90 H to 0.66 H and the change of negative capacitance values from -142.42 nF to -134.23 nF respectively, as is apparent from Tables 8, 10, and 12. Therefore, when the negative capacitance-inductance shunt is to be used for vibration suppression, it is recommended that both the negative capacitor values and the inductor values are changed when the focus is on low frequency vibration control, while for high frequency vibration suppression, the change of resistor values is more feasible.

5.2 Efficiency of the Negative Capacitance-Inductance Shunt Circuit

As shown above, the shunt model accurately predicts the power output behavior of a negative capacitance-inductance shunt. Therefore, it can be used to investigate the improvement in the shunt efficiency as given by equation (13). As discussed by Beck et al. [27], the efficiency of the shunt can be increased only by decreasing the power output of op-amp as the power output of a shunt cannot change for a desired negative capacitance shunt impedance to produce control. The same methodology is also adopted here for the case of efficiency investigations of the negative capacitance-inductance shunt. Thus, through the use of equation (11), four simulated power output plots of op-amp for the frequency range of interest are plotted as shown in Figs. 24, 25, 26, and 27 respectively. Equation (11) allows

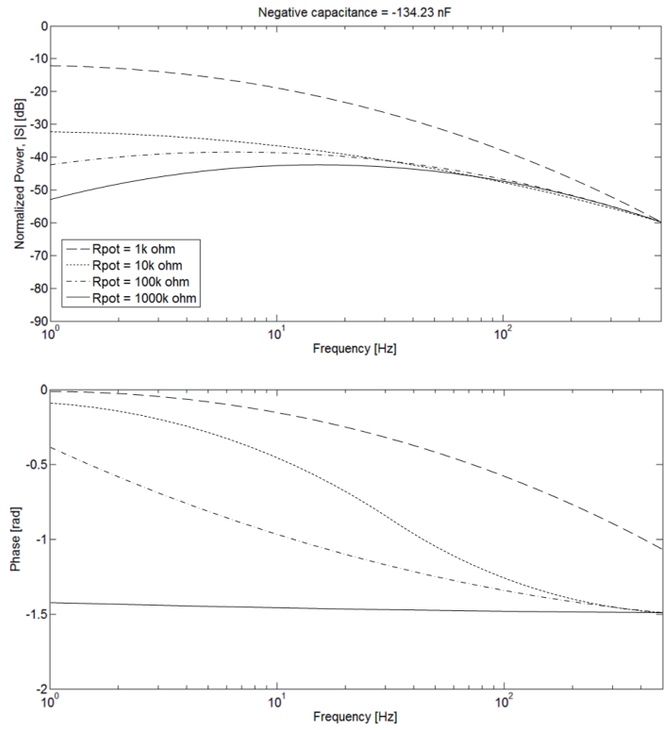

Fig. 24. Simulated normalized power output of the op-amp, amplitude and phase, for four values of potentiometer R_{pot} for full negative capacitance-inductance shunt.

DOI: http://dx.doi.org/10.5139/IJASS.2015.16.2.223

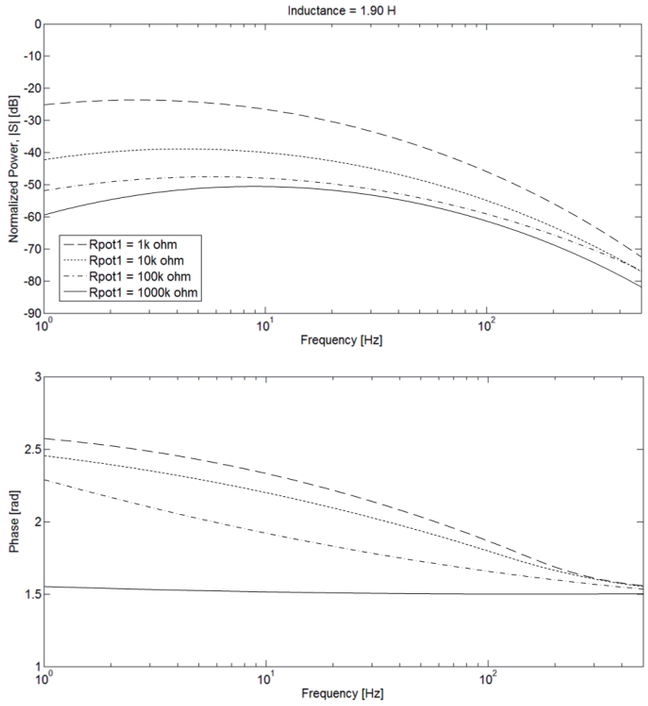

Fig. 25. Simulated normalized power output of the op-amp, amplitude and phase, for four values of potentiometer R_{pot1} for full negative capacitance-inductance shunt.

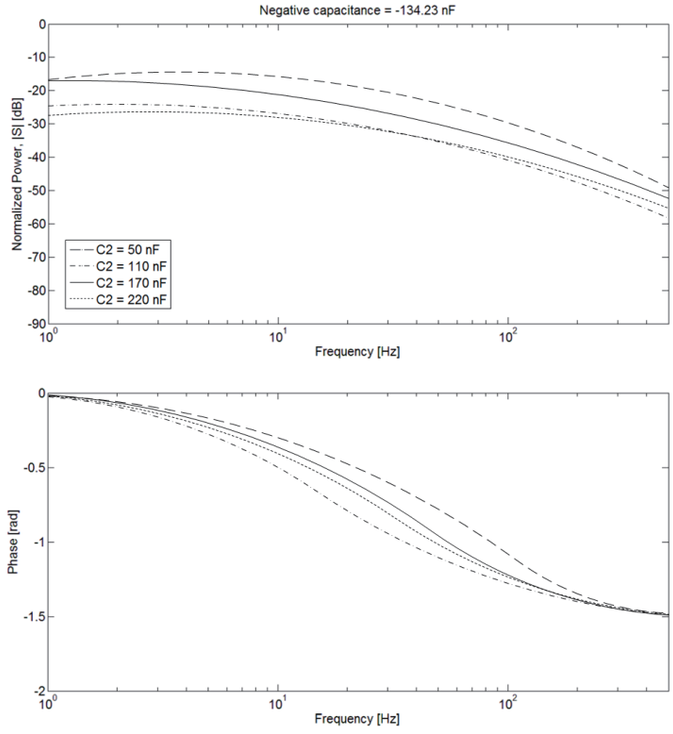

Fig. 26. Simulated normalized power output of the op-amp, amplitude and phase, for four values of reference capacitor C_2 for full negative capacitance-inductance shunt.

us to alter the resistance ratio R_4/R_3, to alter the adjustable resistance R_{13}(Eq. 7), to change the reference capacitance C_2, and to change the capacitance for synthetic inductance, i.e. C_i(Eq. 7), without changing the impedance of the shunt. Therefore, the power output of op-amp will first be investigated by changing the total potentiometer resistance given by Eqs. (20) and (21) as shown below. The effect of changing the reference capacitor C_2 and capacitance for synthetic inductance, i.e. C_i, on the power output of op-amp will then be investigated for the improvement of negative capacitance-inductance shunt efficiency. These investigations are performed using a resistance of 300 ohm, an inductance of 1.90 H, and a negative capacitance of -134.23 nF.

$$R_{pot} = R_3 + R_4 \tag{20}$$

$$R_{pot1} = R_{10} + R_{11} + R_{12} + R_{13} \tag{21}$$

Figure 24 shows that power changes significantly by changing the values of R_{pot}, with the maximum potentiometer i.e. 1000k ohm giving the least power output. The phase plot of the power for this potentiometer is also close to that of an ideal negative capacitor i.e. -π/2 rad. Similarly, from Fig. 25 it is clear that the power changes significantly by reducing the values of R_{pot1} with the maximum potentiometer, i.e. 1000k ohm, giving the least power output. The phase plot of the power for this potentiometer is also close to that of an ideal inductor i.e. π/2 rad. The power output for four values of reference capacitor C_2 and four values of capacitance for synthetic inductance C_i is shown in Figs. 26 and 27 respectively. From Figs. 26 and 27, it is clear that C_2 and C_i do not change the power output of the op-amp as much as the potentiometers R_{pot} and R_{pot1}. Fig. 26 indicates that although a 220 nF reference capacitor has the lowest power output for the full negative capacitance-inductance shunt system, the 110 nF reference capacitor still has a phase that is closest to -π/2 rad for all frequencies. Fig. 27 indicates that a 100 nF capacitor has the lowest power output with the phase also closest to π/2 rad for the frequency range of interest. Therefore, in order to achieve the higher power output efficiency of a negative capacitance-inductance shunt, it is necessary to use higher potentiometer values while the values of the reference capacitor and the capacitor for the synthetic inductance should be kept near to the patch capacitance.

5.3 Limitations of the Negative Capacitance-Inductance Shunt Circuit

As the negative capacitance-inductance shunt circuit

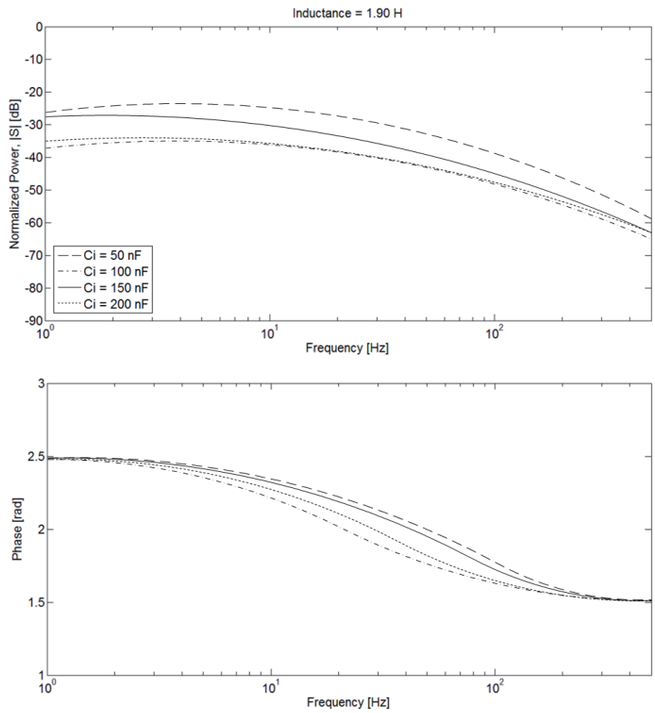

Fig. 27. Simulated normalized power output of the op-amp, amplitude and phase, for four values of reference capacitor C_i for full negative capacitance-inductance shunt.

DOI: http://dx.doi.org/10.5139/IJASS.2015.16.2.223

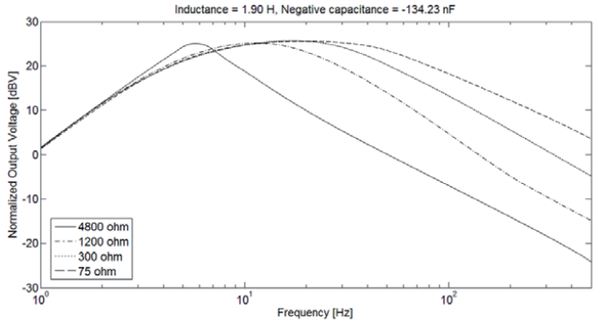

Fig. 28. Simulated normalized voltage output of the op-amp for four values of series resistance R_s for full negative capacitance-inductance shunt.

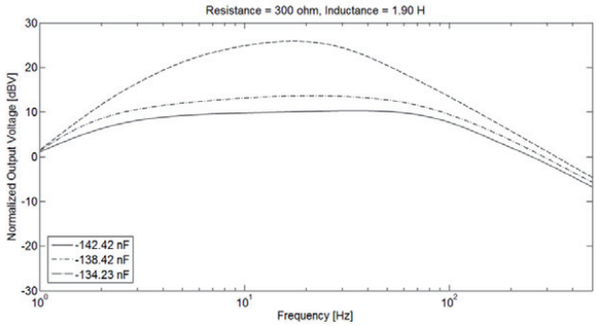

Fig. 29. Simulated normalized voltage output of the op-amp for three values of negative capacitance C_n for full negative capacitance-inductance shunt.

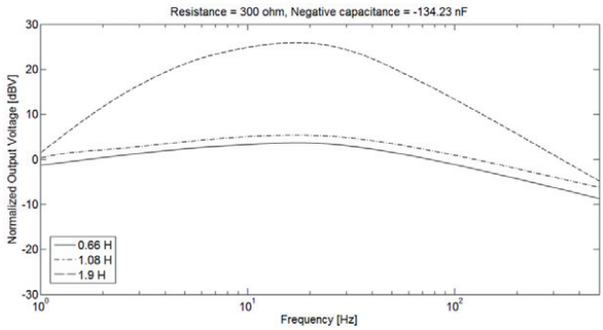

Fig. 30. Simulated normalized voltage output of the op-amp for three values of series inductance L_s for full negative capacitance-inductance shunt.

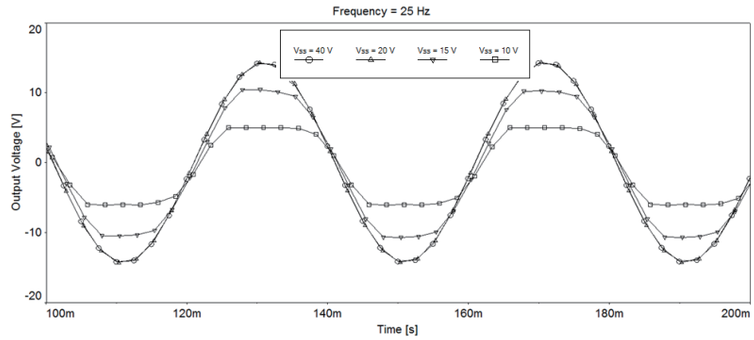

Fig. 31. Op-amp voltage output for four values of power supply voltage.

modeled the behavior of the op-amp accurately, it is important to determine its limitations to achieve a linear response for a given disturbance. Fig. 28 shows the normalized output voltage of op-amp verses frequency for four values of series resistance R_s at a constant inductance of 1.90 H and negative capacitance of -134.23 nF. The maximum value of the output voltage moves to a higher frequency with the decrease in the series resistance values. Also, the peak values of all the resistances are observed to be the same. Fig. 29 shows the normalized output voltage of op-amp versus frequency for three values of negative capacitance C_n at a constant series resistance of 300 ohm and series inductance of 1.90 H. The output voltage increases with the decrease in the negative capacitance values. It peaks exponentially for the negative capacitance value, which is closer to the piezoelectric patch capacitance. Fig. 30 shows the normalized output voltage of op-amp versus frequency for three values of series inductance L_s at a constant series resistance of 300 ohm and negative capacitance of -134.23 nF. The output voltage increases with the increase in the series inductance values, and peaks exponentially for the inductance of 1.90 H. Therefore, in conclusion, the voltage response of the op-amp is more sensitive to the changes in the negative capacitance and series inductance values than the changes in the series resistance values. Also, in order to determine the peak output voltage of the op-amp, it is recommended to refer to the negative capacitance and series inductance values rather than to the series resistance values. For this purpose, the value of negative capacitance that is closer to the piezoelectric patch capacitance C_p and the largest series inductance value will always give better results in terms of maximum op-amp voltage output.

The power supplied to the op-amp for its operation is also important to obtain a proper response of the negative capacitance-inductance shunt circuit. Since we used linear and harmonic assumptions for our analysis of the circuit response, as shown in Fig. 31, the response of the circuit may become nonlinear if the op-amp output voltage approaches the supply voltage V_{ss} because of the output voltage limit of op-amp. Fig. 31 shows the output voltage of op-amp for four values of supply voltage V_{ss} at a single frequency of 25 Hz. For the supply voltage of 40 V and 20 V, the response is normal; however, when the supply voltage is decreased to 15 V, the amplitude of the response decreases due to the clipping effect. For the 10 V power supply, the circuit behaves like an unstable circuit. Therefore, when a negative capacitance-inductance shunt is to be used for control of broadband disturbances, it is important to use a circuit model to determine its proper parameters and the supply voltage in order to achieve a linear response with better control performance.

6. Conclusion

A negative capacitance-inductance shunt was modeled and verified experimentally for vibration control of a piezostructure under broadband excitations. The power output and efficiency of the shunt were fully investigated and discussed. It was shown that the power output of op-amp is accurately predicted by a circuit model of a piezoelectric patch connected to a negative capacitance-inductance shunt. The negative capacitance-inductance shunt was also compared to the negative capacitance shunt to show its better performance for the control of a cantilever beam subjected to wideband frequency disturbances. Moreover, it was shown that the efficiency of the negative capacitance-inductance shunt can be improved by determining the optimal potentiometer, while keeping the reference capacitor and capacitor for synthetic inductor values closer to that of the piezoelectric patch capacitance. The model also predicted the output voltage limits of op-amp against the supply voltage to obtain a linear response for a given disturbance.

Acknowledgments

This work was sponsored by the Qing Lan Project and a Project funded by the(PAPD). The authors are also grateful to the Fundamental Research Funds of the Central Universities (No. NS2013010).

References

[1] Hopkins, M.A., Henderson, D.A., Moses, R.W., Ryall, T., Zimcik, D.G. and Spangler, R.L., "Active vibration suppression systems applied to twin-tail buffering", *Proc. SPIE Smart Structures and Materials: Industrial and Commercial Application of Smart Structures Technologies*, Vol. 3326, 1998, pp.27-33.

DOI:10.1117/12.310663.

[2] Simpson, J. and Schweiger, J., "Industrial approach to piezoelectric damping of large fighter aircraft components", *Proc. SPIE Smart Structures and Materials: Industrial and Commercial Application of Smart Structures Technologies*, Vol. 3326, 1998, pp. 34-46. DOI:10.1117/12.310669.

[3] Kim, S., Han, C. and Yun, C., "Improvement of

aeroelastic stability of hingeless helicopter rotor blade by passive piezoelectric damping", *Proc. SPIE Smart Structures and Materials: Passive Damping and Isolation*, Vol. 3672, 1999, pp. 131-141. DOI:10.1117/12.349776.

[4] Wu, S., Turner, T.L. and Rizzi, S.A., "Piezoelectric shunt vibration damping of an F-15 panel under high-acoustic excitation", *Proc. SPIE Smart Structures and Materials: Damping and Isolation*, Vol. 3989, 2000, pp. 276-287.

DOI:10.1117/12.384568.

[5] Sheta, E.F. and Moses, R.W., "Active smart material control system for buffet alleviation", *Journal of Sound and Vibration*", Vol. 292, No. 3-5, 2006, pp.854-868.

DOI:10.1016/j.jsv.2005.09.002.

[6] Davis, C.L. and Lesieutre, G.A., "A modal strain energy approach to the prediction of resistivity shunted piezoceramic damping", *Journal of Sound and Vibration*, Vol. 184, No. 1, 1995, pp. 129–139.

DOI: 10.1006/jsvi.1995.0308.

[7] Forward, R.L., "Electronic damping of vibrations in optical structures", *Applied Optics*, Vol. 18, No. 5, 1979, pp. 690-697.

DOI:10.1364/AO.18.000690.

[8] Hagood, N.W. and von Flotow, A., "Damping of structural vibrations with piezoelectric materials and passive electrical networks", *Journal of Sound and Vibration*, Vol. 146, No. 2, 1991, pp. 243-268.

DOI:10.1016/0022-460X(91)90762-9.

[9] Qureshi, E.M., Shen , X. and Chen J.J., "Vibration control laws via shunted piezoelectric transducers: A review", *International Journal of Aeronautical and Space Sciences*, Vol. 15, No. 1, 2014, pp. 1-19.

DOI:10.5139/IJASS.2014.15.1.1.

[10] Wu, S.Y., "Piezoelectric shunts with a parallel R-L circuit for structural damping and vibration control", *In Proc. SPIE Symp. Smart Structures Materials Passive Damping Isolation*, *May* 1, Vol. 2720, 1996, pp. 259-269.

DOI:10.1117/12.239093.

[11] Hollkamp, J.J. and Gordon, R.W., "An experimental comparison of piezoelectric and constrained layer damping", *Smart Materials and Structures*, Vol. 5, 1996, pp. 715-722.

DOI:10.1088/0964-1726/5/5/019.

[12] Caruso, G., "A critical analysis of electric shunt circuits employed in piezoelectric passive vibration damping", *Smart Materials and Structures*, Vol. 10, 2001, pp. 1059-1068.

DOI:10.1088/0964-1726/10/5/322.

[13] Spadoni, A., Ruzzene, M. and Cunefare, K., "Vibration and wave propagation control of plates with periodic arrays of shunted piezoelectric patches", *Journal of Intelligent Material Systems and Structures*, Vol. 20, No. 8, 2009, pp.979-990. DOI:10.1177/1045389X08100041.

[14] Hollkamp, J.J., "Multimodal passive vibration suppression with piezoelectric materials and resonant shunts", *Journal of Intelligent Material Systems and Structures*, Vol. 5, No. 1, 1994, pp. 49-56.

DOI:10.1177/1045389X940050010-6.

[15] Wu, S-Y., "Method for multiple mode piezoelectric shunting with single PZT transducer for vibration control", *Journal of Intelligent Material Systems and Structures*, Vol. 9, 1998, pp. 991-998.

DOI:10.1177/1045389X980090120-4.

[16] Behrens, S., Moheimani, S.O.R. and Fleming, A.J., "Multiple mode current flowing passive piezoelectric shunt controller", *Journal of Sound and Vibration*, Vol. 266, No. 5, 2003, pp. 929-942.

DOI:10.1016/S0022-460X(02)0138-0-9.

[17] Niederberger, D., Fleming, A.J., Moheimani, S.O.R. and Morari, M., "Adaptive multi-mode resonant piezoelectric shunt damping", *Smart Materials and Structures*, Vol. 13, No. 5, 2004, pp. 1025-1035.

DOI: 10.1088/0964-1726/13/5/007.

[18] dell'Isola, F., Maurini, C. and Porfiri, M., "Passive damping of beam vibrations through distributed electric networks and piezoelectric transducers: prototype design and experimental validation", *Smart Materials and Structures*, Vol. 13, No. 2, 2004, pp. 299-308.

DOI:10.1088/0964-1726/13/2/008.

[19] Park, C.H. and Baz, A., "Vibration control of beams with negative capacitive shunting of interdigital electrode piezoceramics", *Journal of Vibration and Control*, Vol. 11, 2005, pp. 331-346.

DOI: 10.1177/107754605040949.

[20] Wu, S-Y., "Broadband piezoelectric shunts for passive structural vibration control", *Proc. SPIE 4331, Smart Structures and Materials 2001: Damping and Isolation, July* 2, 2001, pp. 251-261.

DOI: 10.1117/12.432708.

[21] Behrens, S., Fleming, A.J. and Moheimani, S.O.R., "New method for multiple-mode shunt damping of structural vibration using a single piezoelectric transducer", *SPIE-Smart Structures and Materials 2001 (Newport Beach, CA), July 2*, 2001, pp. 239–250.

DOI: 10.1117/12.432707.

[22] Wu, S-Y., "Broadband piezoelectric shunt for structural vibration control", *US Patent* 6,075,303, 2000.

[23] Behrens, S., Fleming, A.J. and Moheimani, S.O.R., "A broadband controller for shunt piezoelectric damping of structural vibration", *Smart Materials and Structures*, Vol. 12, 2003, pp. 18–28.

DOI: 10.1088/0964-1726/12/1/303.

[24] Tang, J. and Wang, K.W., "Active-passive hybrid

piezoelectric networks for vibration control: Comparisons and improvement", *Smart Materials and Structures*, Vol. 10, No. 4, 2001, pp. 794-806.

DOI:10.1088/0964-1726/10/4/325.

[25] Bisegna, P., "On the use of negative capacitances for vibration damping of piezoactuated structures", *Proc. SPIE 5760, Smart Structures and Materials 2005: Damping and Isolation*, *16 May*, 2005, pp. 317-328.

DOI:10.1117/12.600885.

[26] De Marneffe, B. and Preumont, A., "Vibration damping with negative capacitance shunts: theory and experiment", *Smart Materials and Structures*, Vol. 17, No. 3, 2008, pp. 035015.

DOI:10.1088/0964-1726/17/3/0350-15.

[27] Beck, B.S., Cunefare, K.A. and Manuel, C., "The power output and efficiency of a negative capacitance shunt for vibration control of a flexural system", *Smart Materials and Structures*, Vol. 22, No. 6, 2013, pp. 065009.

DOI:10.1088/0964-1726/22/6/0650-09.

[28] Horowitz, P. and Hill, W., *The Art of Electronics*, Cambridge University Press, New York, 1996.

[29] Riodan, R.H.S., "Simulated inductors using differential amplifiers", *Electronic Letter*, Vol. 3, No. 2, 1967, pp. 50-51.

DOI:10.1049/el:19670039

[30] Cunefare, K.A., "Negative capacitance shunts for vibration suppression: wave based tuning and reactive input power", *Active (Adelaide)*, 2006.

[31] Beck, B., Cunefare, K.A., and Ruzzene, M., "Broadband vibration suppression assessment of negative impedance shunts", *SMASIS08 (Ellicott City, MD)*, 2008.

DOI: http://dx.doi.org/10.5139/IJASS.2015.16.2.223